Published in final edited form as:
ACS Nano. 2022 January 25; 16(1): 1409–1420. doi:10.1021/acsnano.1c09456.

Potential-Independent Intracellular Drug Delivery and Mitochondrial Targeting

Yin Liu,
Department of Pharmaceutical Sciences, Irma Lerma Rangel College of Pharmacy, Texas A&M University, College Station, Texas 77843, United States; School of Environment, Hangzhou Institute for Advanced Study, UCAS, Hangzhou, Zhejiang Province 330106, China

Jian Zhang,
Department of Pharmaceutical Sciences, Irma Lerma Rangel College of Pharmacy, Texas A&M University, College Station, Texas 77843, United States

Ying Tu,
Department of Pharmaceutical Sciences, Irma Lerma Rangel College of Pharmacy, Texas A&M University, College Station, Texas 77843, United States

Lin Zhu
Department of Pharmaceutical Sciences, Irma Lerma Rangel College of Pharmacy, Texas A&M University, College Station, Texas 77843, United States

Abstract

In this study, two types of the fluoroamphiphile analogs were synthesized and self-assembled into the "core–shell" micellar nanocarriers for intracellular delivery and organelle targeting. Using the fluorescent dyes or vitamin E succinate as the cargo, the drug delivery and targeting capabilities of the fluoroamphiphiles and their micelles were evaluated in the cell lines, tumor cell spheroids, and tumor-bearing mice. The "core-fluorinated" micelles exhibited favorable physicochemical properties and improved the cellular uptake of the cargo by around 20 times compared to their "shell-fluorinated" counterparts. The results also indicated that the core-fluorinated micelles underwent an efficient clathrin-mediated endocytosis and a rapid endosomal escape thereafter. Interestingly, the internalized fluoroamphiphile micelles preferentially accumulated in mitochondria, by which the efficacy of the loaded vitamin E succinate was boosted both *in vitro* and *in vivo*. Unlike the popularly used cationic mitochondrial targeting ligands, as a charge-neutral nanocarrier, the fluoroamphiphiles' mitochondrial targeting was potential independent. The mechanism study suggested that the strong binding affinity with the phospholipids, particularly

---

Corresponding Author: Lin Zhu – Department of Pharmaceutical Sciences, Irma Lerma Rangel College of Pharmacy, Texas A&M University, College Station, Texas 77843, United States; lzhu@tamu.edu.

Supporting Information
The Supporting Information is available free of charge at https://pubs.acs.org/doi/10.1021/acsnano.1c09456.
Details of the materials and methods; synthesis and characterization of fluoroamphiphiles (Figures S1–S10); cellular uptake and intracellular localizations of the micelles (Figures S11–S24); *in vitro* and *in vivo* anticancer activity (Figures S25–28) (PDF)
Video S1: Intracellular localization of the Rh-PE-labeled PEG2k-F7 micelles in the mitochondria, ER, and Golgi apparatus (MP4)

Complete contact information is available at: https://pubs.acs.org/10.1021/acsnano.1c09456

The authors declare no competing financial interest.

the cardiolipin, played an important role in the fluoroamphiphiles' mitochondrial targeting. These charge-neutral fluoroamphiphiles might have great potential to be a simple and reliable tool for intracellular drug delivery and mitochondrial targeting.

Graphical Abstract

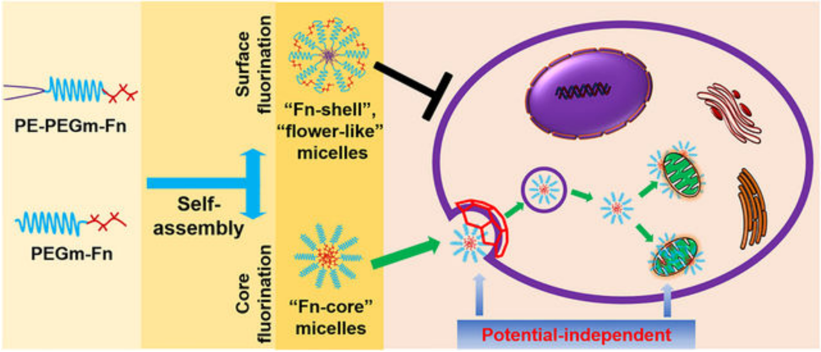

Keywords

mitochondrial targeting; intracellular drug delivery; fluoroamphiphiles; polymeric micelles; potential independent; cancer targeting

Targeted delivery of therapeutics and diagnostics to the specific tissues, cells, and even intracellular compartments/organelles has attracted increasing interest.[1] Mitochondria, a key organelle, are cells' powerhouses and metabolic signaling centers, supporting a wide range of physiological and pathological processes of mammalian cells. Mitochondrial health is critical, and their defects or dysfunctions have been connected with many human diseases and disorders, such as neurological diseases, cardiovascular diseases, and cancer.[2] Mitochondria have become one of the most important therapeutic targets and the specific delivery of therapeutics or imaging probes to mitochondria is highly desirable for studying mitochondrial functions and treating mitochondria-related diseases.[3]

However, because of the hydrophobicity, dense double membranes, and negative potential, mitochondria are difficult-to-access for many therapeutics.[3] Over the past decade, significant effort has been made to develop the mitochondria-targeted systems for delivery of drugs and imaging agents. Among them, the cationic targeting ligands, including the triphenylphosphonium (TPP)-based cations, rhodamine 123 (Rh123), cyanine cations, and cationic peptides, have been developed to modify drug molecules or their carriers to enhance their binding affinity with the "negatively charged" mitochondria.[3,4] For example, the TPP has been successfully conjugated with various drugs including vitamin E succinate (VES), coenzyme Q10, and tamoxifen, to create the mitochondria-targeted drug conjugates, that is, MitoVES,[5,6] MitoQ,[7] and MitoTam,[8] respectively. Some of these conjugates have been used in clinics. However, the positive charge-induced strong ionic interactions may cause nonspecific biodistribution and undesirable side effects.[9] On the other hand, the potential-driven mitochondrial targeting would be compromised if mitochondria undergo depolarization during the cell apoptosis or drug treatments.[6,10,11] A mitochondrial targeting strategy which can tackle these issues is needed.

Due to the unique properties, fluorine has been exploited extensively in drug discovery and development to increase the therapeutic activity and the chemical or metabolic stability of numerous drugs.[12] In fact, more than 20% of the marketed drugs, including half of the top drugs sold, contain fluorine. Fluorination is also an effective technique to improve the stability and specificity of proteins[13] and to prepare the molecular probes for the magnetic resonance imaging[14] and positron emission tomography imaging.[15] Recently, various fluoropolymers and other fluorinated biomaterials have been developed and investigated in biomedical applications.[16] Some of the materials have been used as the carriers for cytosolic delivery of nucleic acids, proteins, and peptides.[17–22]

In this study, we synthesized and compared two types of the fluoroamphiphile analogs, phosphatidylethanolamine-polyethylene glycol-fluorocarbon (PE-PEGm-Fn) and polyethylene glycol-fluorocarbon (PEGm-Fn), which could be self-assembled into the “shell-fluorinated” micelles and “core-fluorinated” micelles, respectively. Compared to the triblock PE-PEGm-Fn polymers, the diblock PEGm-Fn polymers were superior as a mitochondria-targeted nanocarrier. The PEGm-Fn’s cellular uptake, intracellular distribution, particularly mitochondrial binding and accumulation, and underlying mechanisms were studied. Furthermore, using the VES as a model drug, the PEGm-Fn’s capabilities of drug delivery and mitochondrial targeting were evaluated in the cell lines, tumor cell spheroids, and tumor-bearing mice.

RESULTS AND DISCUSSION

Fluorination Strategies: Shell Fluorination *vs* Core Fluorination.

In this study, through the design of the fluoroamphiphiles, two nanoparticle fluorination strategies, that is, the shell/surface fluorination and core fluorination, were explored (Figure 1A). The triblock polymers (PE-PEGm-Fn) and diblock polymers (PEGm-Fn) were synthesized (Figure S1) and self-assembled into the “Fn-shell” micelles with a fluorinated shell and the “Fn-core” micelles with a fluorinated core, respectively. To study the influence of the hydrophobic or hydrophilic segments on the properties of the fluoroamphiphiles, various perfluorinated carbons, Fn (n = 3, 5, 7, or 9), and linear PEGm (m = 1k, 2k, and 5k Da) were used to synthesize the polymers. Although many drugs and biomaterials contained fluorine,[12,17,18] the concerns existed regarding the potential toxicity of the highly fluorinated materials, for example, PFOS ($C_8HF_{17}O_3S$) and PFOA ($C_8HF_{15}O_2$).[23] Here, only the low molecular weight Fn segments were used, which have been proven to be safe.[17,18]

To compare the fluorination strategies, only the PEG2k, the mostly investigated PEG in drug delivery,[24] was used to synthesize the aforementioned triblock and diblock fluoroamphiphiles. Due to the small hydrophobic segment (F3), the PEG2k-F3 could not be self-assembled into a stable nanoparticle, as evidenced by the lack of a critical micelle concentration (CMC). All other fluoroamphiphiles could be readily self-assembled into the nanoparticles with the low CMC values (1–100 mg·L^{-1} for PE-PEG2k-Fn and 0.65–2.5 mg·L^{-1} for PEG2k-Fn) (Figure 1B,C). The PEG2k-Fn micelles were uniform and relatively smaller (mean particle size: 100–120 nm) than the PE-PEG2k-Fn micelles (except PE-PEG2k-F9). Because of the outer PEG layer, the PEG2k-Fn micelles had a near neutral ζ potential. For the PE-PEG2k-Fn polymers, however, their mean particle sizes increased from ~120 nm to ~200 nm along with the decrease in their ζ potentials from ~ −20 mV to ~ −30 mV when the fluorination degree (n) increased from 3 to 7. Interestingly, the PE-PEG2k-F9 micelles had a dramatically decreased size (~50 nm) and a near neutral ζ potential (Figure 1D–G). The results suggested that the triblock polymer, PE-PEG2k-Fn, might not have the similar conformation as the diblock polymer, PEG2k-Fn, in the assembled nanoparticles. Due to the hydrophobic interaction, the Fn might have a propensity to move toward the micelle (PE) core resulting in the PEG's outward folding (as opposed to the micelle core) and partially or completely hidden Fn. When the Fn segment was small ($n < 9$), it was able to "protrude" out of the micelles' surface to some extent; however, when the Fn was big enough ($n \geq 9$), the Fn's hydrophobicity overwhelmed the PEG's hydrophilicity resulting in the polymer's complete, "U-shaped" folding. Hypothetically, the PE-PEG2k-Fn assembled micelles might adopt a "flower-like" arrangement[25] (Figure 1A).

To study the cellular uptake of these fluoroamphiphiles, the PEG2k-PE micelles, one of the mostly investigated micellar nanocarriers,[26] were used as the control. The lissamine rhodamine B-phosphatidylethanolamine (Rh-PE) was used as a fluorescent probe to label the micellar nanoparticles. Although, in recent studies, the shell fluorination strategy improved the cell internalization of the "stable" nanoparticles, such as gold nanoparticles[27,28] and dendrimers,[17,29] our microscopy and flow cytometry data indicated that the Fn-core micelles showed much higher cellular uptake (~20-fold higher) than their Fn-shell counterparts (Figure 1H,I). The fluorescence resonance energy transfer (FRET) data showed that the PEG2k-Fn micelles induced the rapid interaction with the lipid bilayer (cell membrane), triggering the efficient cellular uptake, while the PE-PEG2k-Fn's outward-folding PEG chain reduced the micelles' interaction with the lipid bilayer (Figure S2), inhibiting cellular uptake, in agreement with the previous report on "flower-like" micelles.[25] In addition, the Fn-shell micelles (except PE-PEG2k-F9) had greater CMC values and broader mean particle sizes than the Fn-core micelles (Figure 1B–E), indicating the Fn-shell micelles' relatively low stability. The low micelle stability might also interfere the Fn-shell micelles' cellular uptake. The data confirmed that the "core–shell" nanoparticles' performance was influenced not only by the hydrophilic shell but also by the hydrophobic core.[30]

PEGm-Fn Fluoroamphiphiles and Their Self-Assembled Micelles.

Due to the favorable physicochemical properties and improved cellular uptake (Figure 1), a series of the diblock PEGm-Fn fluoroamphiphiles were further synthesized (PEG2k-F7 as an example). The successful fluorination of the PEG slowed down the PEG's shift in the thin-layer chromatography (TLC) (Figure S3). In the ^{1}H-nuclear magnetic resonance (^{1}H NMR) spectra, the amide hydrogen (−NHCO−) and a few other hydrogens near the F7 moiety were detected when the polymer was dissolved in the DMSO-d_6 (Figure S4A), while these peaks disappeared when D_2O or CD_3OD was used as the solvent (Figure S4B,C) indicating the formation of the "core–shell" structure[31] in these solvents, in agreement with the PEGm-Fn's self-assembly and micelle formation data (Figure 1). After fluorination, the F7-Cys was added to the PEG2k, showing an increase of ~320 Da in the molecular weight determined by the matrix-assisted laser desorption ionization-time-of-flight mass spectrometry (MALDI-TOF MS) (Figure S5). In addition to the PEG2k, the PEG1k and PEG5k were used to synthesize the PEGm-Fn fluoroamphiphiles. The PEGm-Fn micelles showed not only the low CMC (Figure S6) and small particle size (Figure S7) but also the high stability at various pHs and even in methanol (Figure S8), a solvent for disrupting the polymeric micelles.[32,33] This was also reflected by the PEGm-Fn's NMR spectra regarding the micelle formation in the CD_3OD (Figure S4C). The high nanoparticle stability was mostly due to the strong fluorocarbon–fluorocarbon interaction[34] and PEG's hydrophilicity.[35] Unlike the cation-based delivery systems,[3] the PEGm-Fn-assembled micelles with the outer PEG shell were near neutral (between −5 and +5 mV) in aqueous environments (Figures 1G and S9), suggesting that they would have good biocompatibility in biomedical applications, particularly drug delivery.[9] Here, a slight shift in the ζ potential was observed when the pH changed from 5.0 to 8.5 (Figure S9), probably due to the PEGm-F7's pK_a (~8.1 ± 0.6, estimated by the ACD/I-Lab 2.0). In a long-term stability (FRET) study, no significant dye "leakage" from the dye-loaded PEGm-Fn micelles has been observed in the aqueous buffers or mouse serum at 37 °C for at least 24 h (Figure S10), ensuring the PEGm-Fn micelles' cargo loading and delivery capability.

Cellular Uptake and Intracellular Delivery.

Recently, the fluorinated cationic materials, such as dendrimers and polyethylenimines, have been developed for intracellular delivery of genes and proteins.[17–19] In this study, high uptake was observed in all PEGm-F7 (m = 1k, 2k, or 5k) assembled micelles in both the normal (NIH/3T3) and cancer cells, including the drug-sensitive (HeLa) and multidrug-resistant (NCI/ADR-RES) cells (Figures 2A and S11), consistent with the uptake of the PEG2k-Fn (n = 5, 7, or 9) micelles (Figure 1H,I). The data implied that the uptake of the PEGm-Fn micelles was most likely independent of the cell type. Compared to the PEG1k-F7 and PEG5k-F7, the PEG2k-F7 had a slightly higher cellular uptake, probably due to the proper balance between the hydrophilicity (of the PEG) and hydrophobicity (of the fluorocarbon).[36] The use of the PEG2k-F7 to modify the PEG2k-PE micelles significantly increased the cellular uptake, which was similar to those of the micelles modified with the trans-activating transcriptional activator (TAT) peptide (Figure S12), a well-known intracellular delivery ligand.[37] The data confirmed that even as a micelle core, the Fn had a considerable impact on the fluoroamphiphiles' biointeractions. Previous studies showed that the fluorocarbons and fluoroamphiphiles could exert a "cholesterol-like" condensing effect on the lipid bilayer/membrane,[38,39] allowing to orient the lipids' polar head groups toward the fluoroamphiphiles. This unique property might facilitate the interaction of the PEGm-Fn with cell membrane (Figures 2D and S2), to trigger the efficient cellular uptake (Figures 1H,I and 2A).

We found that the uptake of the PEG2k-F7 micelles at 4 °C was only about 50% of that at 37 °C, suggesting that the uptake process needed energy. The uptake of the PEG2k-F7 micelles was significantly inhibited by chlorpromazine,[40] an inhibitor of clathrin-mediated endocytosis, rather than the inhibitors (nystatin[41] and 2-hydroxypropyl-β-cyclodextrin[42]) of the caveolae- or lipid raft-mediated endocytosis (Figures 2B and S13). In the dynamic study, the Rh-PE-labeled PEG2k-F7 micelles (red) were initially colocalized with the endosomes (green), showing a yellow-orange fluorescence, and then, the red and green fluorescence were separated each other (Figure 2C). All the results suggested that the PEG2k-F7 micelles might undergo an energy-dependent clathrin-mediated endocytosis and a rapid endosomal escape thereafter. These features would protect the loaded cargoes from the endolysosomal degradation and facilitate the intracellular delivery and organelle targeting.[43] However, we could not rule out the nonendocytic internalization of the PEG2k-F7 micelles,[44] which might account for the moderate cellular uptake at 4 °C (Figure 2B). Further studies indicated that the PEG2k-F7 could induce the quick lipid membrane fusion at both pH 7.4 and pH 5.0 and reached the equilibrium (when the curves level off) in an hour (Figure 2D), while it took more than 20 h for the PEG2k-PE to reach the lipid fusion equilibrium (Figure S14). The lipid fusion/interaction property of the PEG2k-F7 might shed some light on its rapid uptake and efficient endosomal escape.[45]

To track the nanocarrier and cargo, the Rh-PE, as a cargo, was loaded to the fluorescein isothiocyanate (FITC)-PEG2k-F7 assembled micelles. We found that, during the intracellular transport, the cargoes and micelles were colocalized and no obvious cargo leakage was observed (Figure 2E). It was reported that some fluoroamphiphiles were capable of incorporating into the lipid bilayer (membrane) with high affinity.[18,29,46] Our data also showed a strong interaction between the PEG2k-F7 and lipid membrane (Figure 2D). However, due to stronger fluorocarbon–fluorocarbon interaction (*vs* fluorocarbon-hydrocarbon interaction),[34] rather than evenly mixing with the membrane lipids, the fluoroamphiphiles might direct the self-assembly and remain a nanoscale structure within the hydrocarbon environment (lipid membrane).[47] This secured the PEGm-Fn micelle stability during membrane translocation and intracellular transport.

Potential-Independent Mitochondrial Targeting and Underlying Mechanisms.

Though the fluorinated materials/nanoparticles have showed the enhanced cellular uptake,[17,18] their intracellular localization patterns remained vague. Here, we hypothesized that the extreme hydrophobicity of the fluorocarbon (Fn) might favor the fluoroamphiphiles' intracellular distribution in the hydrophobic, membrane-rich organelles, such as mitochondria. To visualize mitochondria, three commercially available mitochondrial dyes, including the MitoView Green (potential-independent, green), rhodamine 123 (Rh123) (potential-dependent, green), and MitoView 633 (potential-dependent, red), were used. The Rh-PE that was proven to have no mitochondrial preference[48] was used as a probe. In accordance with Figure 2C, at as early as 5 min upon incubation, the Rh-PE-labeled PEG2k-F7 micelles (red) were observed on the cell surface, indicating a rapid onset of cell association/uptake (Figure S15). At 30 and 60 min, the micelles were distributed in the intracellular compartments and mainly colocalized with the "green" mitochondria, showing the yellow-orange fluorescence. The similar results were obtained in various cell lines (Figure S16). The zoomed-in images clearly showed that both the FITC-PEG2k-F7 and PEG2k-F7/Rh-PE micelles could accumulate in mitochondria, while the Rh-PE alone had no mitochondrial specificity (Figure S17), consistent with the previous study.[48] In addition to mitochondria and cell nuclei, two more important organelles, the endoplasmic reticulum (ER) and Golgi apparatus, were stained by the ER-Tracker[49] and NBD C6-ceramide,[50] respectively. The PEG2k-F7 micelles showed much lower accumulation in the ER or Golgi apparatus than that in mitochondria, as evidenced by the discrete red and green fluorescence (Figure 3A and Video S1). All these results strongly suggested that the PEG2k-F7 micelles could be quickly internalized and preferentially accumulated in mitochondria. Since the ER and mitochondria may join together at multiple contact sites, so-called the mitochondria-ER associated membranes,[51] a slight ER "colocalization" was observed.

The mitochondrial membrane potential is an important indicator of the mitochondrial health[2] and also a major driving force for cationic ligands to target mitochondria.[3] In this study, the mitochondrial membrane potential was measured by the JC-1 dye. In the cytosol, the JC-1 dye exists as the green fluorescent monomers, while, upon binding to mitochondria, it forms the red fluorescent J-aggregates. A shift from red to green indicates the mitochondrial depolarization.[52] Based on the red/green ratio (Figure 3B), the charge-neutral PEG2k-F7 did not significantly alter the mitochondrial potential, while the cationic TPP or mitochondrial uncoupler, carbonyl cyanide *m*-chlorophenyl hydrazine (CCCP),[53] dramatically depolarized mitochondria. To study the mechanisms of the mitochondrial targeting, the PEG2k, F7, and PE were also labeled by the FITC, respectively, and the mitochondria were stained by the MitoView 633 (red). Both the FITC-PE and FITC-F7 could be efficiently internalized, while the FITC-PEG2k could not enter the cells due to the PEG's "stealth" property (Figure S18). After internalization, the FITC-PE was widely distributed in the cytosol and had no mitochondrial preference, similar to the Rh-PE (Figure S17 and ref 48). In contrast, the FITC-F7 predominantly accumulated in mitochondria (Figure 3C), suggesting that the fluorocarbon (F7) was mainly responsible for the mitochondrial targeting. Upon the mitochondrial isolation from these cells, the mitochondria-associated fluorescent polymers were quantitated. The FITC-F7 showed a doubled mitochondrial accumulation (20.9%) compared to the FITC-PE (11.1%). It was also slightly higher than that of the Rh123 (17.5%) (Figure 3D). The CCCP-induced depolarization substantially reduced the Rh123's (cationic dye) accumulation in mitochondria, but it could not reduce the FITC-F7's mitochondrial accumulation (Figure 3D). The microscopic images also showed that the PEG2k-F7/Rh-PE micelles were able to target mitochondria, although the CCCP changed the mitochondrial potential and morphology (Figure S19). However, the fluorocarbon (Fn) was not suitable as a drug carrier by itself due to its extreme hydrophobicity.[54] Here, the proper length of the PEG balanced the hydrophilic-to-hydrophobic ratio and facilitated the polymers' self-assembly into a core–shell micelle for drug loading.

To study the direct binding between the polymers and mitochondria, the mitochondria were freshly isolated from the untreated cells and characterized in terms of the morphology, reactive oxygen species (ROS) production capacity, and ζ potential[55] (Figure S20). Though being electrically neutral, the FITC-PEG2k-F7 and FITC-F7 both showed strong binding affinities with the isolated mitochondria, which were comparable to those of the commercial dyes (Figures 3E and S21). The FITC-PE had a mild mitochondrial binding affinity, consistent with the Figures 3C,D and S18. The TPP preincubation lowered the mitochondrial binding of the Rh123 by about 50% due to the charge neutralization (Figure 3B), while the PEG2k-F7 preincubation did not influence the Rh123's binding with mitochondria (Figure 3F). It was reported that the cationic ligands, including TPP and Rh123, could effectively target the mitochondria that had a great negative potential and their mitochondrial binding affinity highly depended on the mitochondrial potential.[6] However, the mitochondrial potential is not always constant in the cell life cycle and may be depolarized during the cell apoptosis or pharmacological interventions.[56,57] In such conditions, the potential-driven mitochondrial targeting strategy will be compromised.[6,10] Our data suggested that the PEGm-Fn fluoroamphiphiles could target mitochondria in a potential-independent manner, without influencing the mitochondrial potential or being influenced by the mitochondrial potential.

In light of the high hydrophobicity and lack of the positive charge, most likely, the PEGm-Fn fluoroamphiphiles were able to interact with the mitochondrial hydrophobic structures, such as the membrane phospholipids, resulting in high mitochondrial affinity. The liposomes containing various types of phospholipids were prepared and characterized (Figure S22). After incubation with the fluorescent polymers, the polymer–lipid binding was analyzed by flow cytometry (Figure 3G), a protocol used for studying the protein–lipid interaction.[58] Compared to the Rh123 and FITC-PE, the FITC-F7 showed equal or much stronger binding affinities with all tested phospholipids regardless of their charge. The cationic ligand (Rh123) showed a relatively high affinity only with the negatively charged liposomes, while its affinity with the positively charged DOTAP liposomes was even lower than that of the FITC-PE. In contrast, the FITC-PE showed low-moderate binding affinities with all the liposomes. Among the tested natural phospholipids, the cardiolipin, a mitochondria-exclusive phospholipid,[59] showed the strongest binding affinity with the FITC-F7 (Figure S23). The FITC-F7's lipid binding effect was proportional to the cardiolipin contents in the liposomes (Figure S24). Since both the PEGylation[60] and fluorination[12,61] were reported to reduce the nonspecific interaction with the biomolecules, the strong binding affinity with the phospholipids, particularly the cardiolipin, might play an important role in the fluoroamphiphiles' mitochondrial targeting. However, whether the fluoroamphiphiles could bind to other mitochondrial components, such as specific proteins and nucleic acids, needs to be further studied.

In vitro Drug Delivery.

Here, the vitamin E succinate (VES),[6,62,63] a widely investigated "mitocan" that exerts the anticancer activity by way of mitochondrial "destabilization",[64] was used as a model drug. The VES was loaded to the PEG2k-F7 micelles at a loading efficiency of ~10%. After drug loading, the particle size of the PEG2k-F7 micelles slightly increased (~120 nm) (Figure S25A), while their ζ potential slightly decreased (~ −10 mV) (Figure S25B). The TPP-PEG2k-PE/VES micelles were still positively charged (~ +30 mV). All tested polymeric micelles could hold the VES and significantly prolonged drug release. Compared to the free VES, PEG2k-PE or TPP-PEG2k-PE micelles, the PEG2k-F7 micelles showed relatively slower drug release rate (Figure S25C). This was probably due to the high stability of the PEG2k-F7 micelles.

The PEG2k-F7/VES micelles substantially enhanced the ROS production compared to the free VES and PEG2k-PE/VES micelles (Figure 4A). To study the cytotoxicity, the TPP-modified polymer, TPP-PEG2k-PE, was synthesized to form the potential-dependent cationic micelles[65] as a control. Here, we did not use the TPP-modified VES conjugate

(MitoVES), though it has been widely investigated[6,10] because it is a molecule and cannot form a stable nanoparticle by itself alone. In addition, the MitoVES has a low water solubility and usually needs the corn oil and ethanol mixture as the solvent for drug administration.[6,66] In all tested cell lines, including the drug-resistant cancer cells, the PEG2k-F7/VES micelles showed the highest cytotoxicity among the formulations including the TPP-PEG2k-PE/VES micelles (Figures 4B and S26). In contrast, the free polymers did not show obvious ROS production and cytotoxicity, in agreement with the recent safety reports on the fluorinated biomaterials.[17,18,67]

Since the VES exerts the anticancer activity *via* the mitochondrial complex II (CII),[6,66] the CII activity was measured after treatments. Based on the results (Figure S26C), both the TPP-PEG2k-PE/VES and PEG2k-F7/VES micelles could inhibit the CII activity by around 70%, which almost doubled the inhibitory activity of the free VES or PEG2k-PE/VES micelles. It was worth noting that the positively charged TPP-PEG2k-PE polymers showed a significant CII inhibitory capability (~20%), probably due to the cation-induced mitochondrial depolarization (Figure 3B), while the charge-neutral PEG2k-F7 or PEG2k-PE polymers had no significant influence on the CII activity. It was known that the cardiolipin was mainly located in the inner mitochondrial membrane where the CII also resided.[59] The results confirmed that the PEG2k-F7 micelles were able to carry the cargo (*i.e.*, VES) and translocate across the outer mitochondrial membrane to reach the cardiolipin and CII in the inner mitochondrial membrane. This boosted the efficacy of the loaded VES.

The VES' mitochondrial complex activity inhibition (ref 6 and Figure S26C) would cause mitochondrial depolarization and cell apoptosis,[56,57] which lowered cationic drugs'/dyes' mitochondrial binding (Figure 3F) and accumulation (ref 10 and Figure 3D). Although both the TPP-PEG2k-PE/VES and PEG2k-F7/VES showed the similar CII inhibitory effects after 1 h cell incubation, the lowered mitochondrial binding/accumulation reduced the efficacy of the potential-dependent cationic micelles (TPP-PEG2k-PE/VES) after 48 h cell incubation (Figures 4B and S26A). This would be more significant along with the progressive cell apoptosis during long-term/repetitive drug treatments. In contrast, the charge-neutral PEG2k-F7-mediated mitochondrial targeting and drug delivery were independent of mitochondrial potential, which might greatly benefit the mitochondrial imaging and therapy during anticancer treatments.

Furthermore, a tissue-mimicking tumor cell spheroid model with the well-known "multicellular resistance"[68,69] was developed to challenge the micelles. The PEG2k-F7 micelles (Rh-PE labeled) showed much higher penetration through the spheroids than the PEG2k-PE micelles, as evidenced by the strong spheroid-associated fluorescence (Figure 4C). The PEG2k-F7 micelles' high spheroid penetration enhanced VES' cytotoxicity in the tumor spheroids (Figure 4D) and inhibited the spheroid growth (Figure 4E). The data suggested that the PEG2k-F7-mediated spheroid (tissue) penetration, cellular uptake, and mitochondrial targeting could improve the drugs' efficacy for treating mitochondria-related diseases.

In vivo Biodistribution, Cellular Uptake, and Mitochondrial Accumulation.

Mitochondrial dysfunctions are connected with various types of diseases, including cancer.[70] Unlike the MitoVES' specificity against the fast-proliferating cells with greater mitochondrial potentials (mainly because of the TPP's positive charge),[6] the PEG2k-F7 micelles, as the charge-neutral nanocarriers, were designed to improve the tumor accumulation *via* the enhanced permeability and retention (EPR) effect and to target mitochondria of both cancer cells and cancer supporting cells in the tumor microenvironment.[71]

In the *in vivo* study, the syngeneic 4T1 breast tumor model was generated on the BALB/c mouse which is immunocompetent.[72,73] The immunocompetent mouse model allowed us to study the drug delivery in the presence of the host immune response, a key factor influencing delivery specificity and efficiency.[9] After intravenous (i.v.) injection of the Rh-PE-labeled micelles, the micelles' biodistribution was evaluated according to our previous study.[69] Overall, the PEG2k-F7 micelles showed the high *in vivo* retention. The PEG2k-F7 micelles exhibited a prolonged blood circulation time (Figure 5A), probably because (i) both the PEGylation[60] and fluorination[12,61] could reduce nonspecific biointeractions and (ii) the charge-neutral nanoparticles had longer blood circulating half-lives[9] compared to the charged nanoparticles. Moreover, the appropriate particle size (~100 nm) and high stability ensured the PEG2k-F7 micelles' high accumulation in the 4T1 tumor (Figures 5A,B and S27), a model with a well-known EPR effect.[73,74] Upon the cell dissociation from the tumor tissues, the micelles' uptake by the tumor cells was analyzed by flow cytometry.[31,69] We found that the PEG2k-F7 micelles had higher cellular uptake than the free dye and PEG2k-PE micelles (Figure 5C). To evaluate the micelles' mitochondrial targetability, the mitochondria were further isolated from the dissociated tumor cells, and the mitochondria-associated micelles (dyes) were analyzed by flow cytometry. Compared to the free dye and PEG2k-PE micelles, the PEG2k-F7 micelles showed a higher and persistent accumulation in the tumor cells' mitochondria (Figure 5D). The *in vitro* and *in vivo* mitochondrial targeting data were well correlated.

In vivo Anticancer Activity.

Due to the low solubility and high dose (~400 $mg \cdot kg^{-1}$), the VES or its TPP conjugate (*i.e.*, MitoVES) was usually administered in corn oil containing 4% ethanol *via* the intraperitoneal (i.p.) injection.[6,66] In this study, the VES-loaded PEG2k-F7 micelles were readily dispersed in the PBS and given *via* the i.v. injection to the 4T1 tumor-bearing mice at a low dose (20 $mg \cdot kg^{-1}$). After three injections, all micellar formulations exhibited significant anticancer activities, while the free VES did not show obvious anticancer activity compared to the saline group. On day 14 upon the injection, the PEG2k-F7/VES micelles inhibited the tumor size by ~75% and the tumor weight by ~65% compared to the saline group, while the PEG2k-PE/VES micelles only showed ~40% inhibition in the tumor size and ~30% inhibition in the tumor weight (Figure 6A–C). No significant changes in the mouse body weights (Figure 6D) and white blood cell counts (Figure 6E) among the treatments were observed. Also, the treatments did not significantly influence the functions of liver and kidney (Figure S28). The H&E staining (Figure 6F) indicated that the vital organs had no histological changes after treatments. In the tumor sections, the obvious cell death/necrotic areas were observed in the micelle-treated groups (PEG2k-PE/VES and PEG2k-F7/VES) but not in the free PEG2k-F7 or free VES groups. Compared to the PEG2k-PE/VES, the PEG2k-F7/VES caused more cell death in the tumor. All these data indicated that (i) the free PEG2k-F7 fluoroamphiphiles were safe even after multiple i.v. injections; and (ii) even at a low VES dose, the PEG2k-F7 micelles could substantially boost the VES' anticancer activity without significant adverse effects.

Like many other nanoparticles, in addition to accumulating in the tumor, the PEG2k-F7 micelles were found to accumulate in the mononuclear phagocyte system, such as liver (Figure 5B). It was known that the large fluorocarbons were hardly degraded and eliminated from our body, which might cause toxicity.[23] To address this issue, in this study, only the low molecular weight Fn segments ($n \leq 9$) were used, which have been proven to be safe.[17,18] The safety data of PEG2k-F7 micelles (Figures 4A, 6, S26B,C, and S28) were also supported by previous reports on PEG2k[75] and heptafluorobutyric acid,[17] the potential degradation products/intermediates of PEG2k-F7 polymers.

CONCLUSION

We synthesized various fluoroamphiphiles and explored two fluorination strategies (shell *vs* core fluorination) on the self-assembled micellar nanoparticles. We demonstrated a reliable intracellular delivery and mitochondrial targeting strategy using the diblock fluoroamphiphiles as a nanocarrier. Despite being charge-neutral, the fluoroamphiphile-assembled micelles were efficiently internalized by the cells, escaped from endosomes, and preferentially accumulated in mitochondria. The fluoroamphiphile-mediated mitochondrial targeting was potential independent and could deliver the cargo to mitochondria without compromising mitochondrial health both *in vitro* and *in vivo*. Our findings suggested that the use of the fluoroamphiphiles might be a simple and effective way for targeting of therapeutic and imaging agents to mitochondria. Because of the important roles of mitochondria in various types of diseases, the approach is expected to advance the diagnoses and treatments of not only cancer but also other types of diseases.

MATERIALS AND METHODS

The fluoroamphiphiles were synthesized and their chemical structures were characterized. The self-assembled micelles were characterized by their CMC values, particle sizes, ζ potentials, and morphology. The FRET was performed to study the lipid fusion and micelle stability. The cellular uptake, intracellular localization, and spheroid penetration were determined by flow cytometry, fluorescence microscopy, or confocal microscopy. The binding affinity with the isolated mitochondira or liposomes were determined by flow cytometry. The cytotoxicity was measured by the CellTiter-Blue Cell Viability Assay (Promega). The *in vivo* biodistribution and anticancer activity were studied on the syngeneic orthotopic 4T1 mouse model. A full description of materials and methods is provided in Supporting Information Materials and Methods.

Supplementary Material

Refer to Web version on PubMed Central for supplementary material.

ACKNOWLEDGMENTS

The work was supported by the National Cancer Institute of the National Institutes of Health (R15CA213103) and the National Natural Science Foundation of China (21707159, 22036002). The authors would like to thank the Dr. Zack Abd Elmageed lab (Texas A&M University), Dr. Bing Yan lab (Shandong University), and Dr. Wei Xu lab (Texas A&M University, Corpus Christi) for kind help in the study and also thank Dr. Vladimir P. Torchilin (Northeastern University) for his valuable comments on the manuscript. The authors acknowledge the use of Chemistry Mass Spectrometry Facility and Microscopy and Imaging Center at Texas A&M University.

REFERENCES

(1). Torchilin VP Multifunctional, Stimuli-Sensitive Nano-particulate Systems for Drug Delivery. Nat. Rev. Drug Discovery 2014, 13 (11), 813–827. [PubMed: 25287120]

(2). Nunnari J; Suomalainen A Mitochondria: In Sickness and in Health. Cell 2012, 148 (6), 1145–1159. [PubMed: 22424226]

(3). Zielonka J; Joseph J; Sikora A; Hardy M; Ouari O; Vasquez-Vivar J; Cheng G; Lopez M; Kalyanaraman B Mitochondria-Targeted Triphenylphosphonium-Based Compounds: Syntheses, Mechanisms of Action, and Therapeutic and Diagnostic Applications. Chem. Rev 2017, 117 (15), 10043–10120. [PubMed: 28654243]

(4). Jean SR; Ahmed M; Lei EK; Wisnovsky SP; Kelley SO Peptide-Mediated Delivery of Chemical Probes and Therapeutics to Mitochondria. Acc. Chem. Res 2016, 49 (9), 1893–1902. [PubMed: 27529125]

(5). Dong L-F; Jameson VJ; Tilly D; Prochazka L; Rohlena J; Valis K; Truksa J; Zobalova R; Mahdavian E; Kluckova K; et al. Mitochondrial Targeting of A-Tocopheryl Succinate Enhances Its Pro-Apoptotic Efficacy: A New Paradigm for Effective Cancer Therapy. Free Radicals Biol. Med 2011, 50 (11), 1546–1555.

(6). Dong L-F; Jameson VJ; Tilly D; Cerny J; Mahdavian E; Marín-Hernández A; Hernández-Esquivel L; Rodríguez-Enríquez S; Stursa J; Witting PK; et al. Mitochondrial Targeting of Vitamin E Succinate Enhances Its Pro-Apoptotic and Anti-Cancer Activity *via* Mitochondrial Complex II. J. Biol. Chem 2011, 286 (5), 3717–3728. [PubMed: 21059645]

(7). Kelso GF; Porteous CM; Coulter CV; Hughes G; Porteous WK; Ledgerwood EC; Smith RA; Murphy MP Selective Targeting of a Redox-Active Ubiquinone to Mitochondria within Cells: Antioxidant and Antiapoptotic Properties. J. Biol. Chem 2001, 276 (7), 4588–4596. [PubMed: 11092892]

(8). Rohlenova K; Sachaphibulkij K; Stursa J; Bezawork-Geleta A; Blecha J; Endaya B; Werner L; Cerny J; Zobalova R; Goodwin J; et al. Selective Disruption of Respiratory Super-complexes as a New Strategy to Suppress Her2high Breast Cancer. Antioxid. Redox Signaling 2017, 26 (2), 84–103.

(9). Blanco E; Shen H; Ferrari M Principles of Nanoparticle Design for Overcoming Biological Barriers to Drug Delivery. Nat. Biotechnol 2015, 33 (9), 941–951. [PubMed: 26348965]

(10). Rohlena J; Dong L-F; Kluckova K; Zobalova R; Goodwin J; Tilly D; Stursa J; Pecinova A; Philimonenko A; Hozak P; et al. Mitochondrially Targeted A-Tocopheryl Succinate Is Anti-angiogenic: Potential Benefit against Tumor Angiogenesis but Caution against Wound Healing. Antioxid. Redox Signaling 2011, 15 (12), 2923–2935.

(11). Lyamzaev KG; Tokarchuk AV; Panteleeva AA; Mulkidjanian AY; Skulachev VP; Chernyak BV Induction of Autophagy by Depolarization of Mitochondria. Autophagy 2018, 14 (5), 921–924. [PubMed: 29458285]

(12). Gillis EP; Eastman KJ; Hill MD; Donnelly DJ; Meanwell NA Applications of Fluorine in Medicinal Chemistry. J. Med. Chem 2015, 58 (21), 8315–8359. [PubMed: 26200936]

(13). Yoder NC; Kumar K Fluorinated Amino Acids in Protein Design and Engineering. Chem. Soc. Rev 2002, 31 (6), 335–341. [PubMed: 12491748]

(14). Takaoka Y; Sakamoto T; Tsukiji S; Narazaki M; Matsuda T; Tochio H; Shirakawa M; Hamachi I Self-Assembling Nanoprobes That Display Off/On 19f Nuclear Magnetic Resonance Signals for Protein Detection and Imaging. Nat. Chem 2009, 1 (7), 557–561. [PubMed: 21378937]

(15). Lee E; Kamlet AS; Powers DC; Neumann CN; Boursalian GB; Furuya T; Choi DC; Hooker JM; Ritter T A Fluoride-Derived Electrophilic Late-Stage Fluorination Reagent for Pet Imaging. Science 2011, 334 (6056), 639–642. [PubMed: 22053044]

(16). Lv J; Cheng Y Fluoropolymers in Biomedical Applications: State-of-the-Art and Future Perspectives. Chem. Soc. Rev 2021, 50 (9), 5435–5467. [PubMed: 33687034]

(17). Wang M; Liu H; Li L; Cheng Y A Fluorinated Dendrimer Achieves Excellent Gene Transfection Efficacy at Extremely Low Nitrogen to Phosphorus Ratios. Nat. Commun 2014, 5, 3053. [PubMed: 24407172]

(18). Zhang Z; Shen W; Ling J; Yan Y; Hu J; Cheng Y The Fluorination Effect of Fluoroamphiphiles in Cytosolic Protein Delivery. Nat. Commun 2018, 9 (1), 1377. [PubMed: 29636457]

(19). Liu H; Wang Y; Wang M; Xiao J; Cheng Y Fluorinated Poly(propylenimine) Dendrimers as Gene Vectors. Biomaterials 2014, 35 (20), 5407–5413. [PubMed: 24709522]

(20). Xu J; Lv J; Zhuang Q; Yang Z; Cao Z; Xu L; Pei P; Wang C; Wu H; Dong Z; Chao Y; Wang C; Yang K; Peng R; Cheng Y; Liu Z A General Strategy towards Personalized Nanovaccines Based on Fluoropolymers for Post-Surgical Cancer Immunotherapy. Nat. Nanotechnol 2020, 15 (12), 1043–1052. [PubMed: 33139933]

(21). Cheng Y.-y. Fluorinated Polymers in Gene Delivery. Acta Polym. Sin 2017, 8, 1234–1245.

(22). Rong G; Wang C; Chen L; Yan Y; Cheng Y Fluoroalkylation Promotes Cytosolic Peptide Delivery. Sci. Adv 2020, 6 (33), No. eaaz1774.

(23). Stahl T; Mattern D; Brunn H Toxicology of Perfluorinated Compounds. Environ. Sci. Eur 2011, 23 (1), 38.

(24). Lukyanov AN; Torchilin VP Micelles from Lipid Derivatives of Water-Soluble Polymers as Delivery Systems for Poorly Soluble Drugs. Adv. Drug Delivery Rev 2004, 56 (9), 1273–1289.

(25). Lee ES; Oh KT; Kim D; Youn YS; Bae YH Tumor pH-Responsive Flower-Like Micelles of Poly(L-Lactic Acid)-BPoly(ethylene Glycol)-B-Poly(L-Histidine). J. Controlled Release 2007, 123 (1), 19–26.

(26). Torchilin VP Micellar Nanocarriers: Pharmaceutical Perspectives. Pharm. Res 2006, 24 (1), 1–16. [PubMed: 17109211]

(27). Dass A; Guo R; Tracy JB; Balasubramanian R; Douglas AD; Murray RW Gold Nanoparticles with Perfluorothiolate Ligands. Langmuir 2008, 24 (1), 310–315. [PubMed: 18052299]

(28). Niikura K; Iyo N; Higuchi T; Nishio T; Jinnai H; Fujitani N; Ijiro K Gold Nanoparticles Coated with Semi-Fluorinated Oligo(ethylene Glycol) Produce Sub-100 nM Nanoparticle Vesicles without Templates. J. Am. Chem. Soc 2012, 134 (18), 7632–7635. [PubMed: 22533717]

(29). Lv J; He B; Yu J; Wang Y; Wang C; Zhang S; Wang H; Hu J; Zhang Q; Cheng Y Fluoropolymers for Intracellular and *in Vivo* Protein Delivery. Biomaterials 2018, 182, 167–175. [PubMed: 30121426]

(30). Gref R; Lück M; Quellec P; Marchand M; Dellacherie E; Harnisch S; Blunk T; Müller R 'Stealth' Corona-Core Nanoparticles Surface Modified by Polyethylene Glycol (PEG): Influences of the Corona (PEG Chain Length and Surface Density) and of the Core Composition on Phagocytic Uptake and Plasma Protein Adsorption. Colloids Surf., B 2000, 18 (3–4), 301–313.

(31). Zhu L; Wang T; Perche F; Taigind A; Torchilin VP Enhanced Anticancer Activity of Nanopreparation Containing an MMP2-Sensitive PEG-Drug Conjugate and Cell-Penetrating Moiety. Proc. Natl. Acad. Sci. U. S. A 2013, 110 (42), 17047–17052. [PubMed: 24062440]

(32). Yao Q; Choi JH; Dai Z; Wang J; Kim D; Tang X; Zhu L Improving Tumor Specificity and Anticancer Activity of Dasatinib by Dual-Targeted Polymeric Micelles. ACS Appl. Mater. Interfaces 2017, 9 (42), 36642–36654. [PubMed: 28960955]

(33). Sarisozen C; Vural I; Levchenko T; Hincal AA; Torchilin VP PEG-PE-Based Micelles Co-Loaded with Paclitaxel and Cyclosporine A or Loaded with Paclitaxel and Targeted by Anticancer Antibody Overcome Drug Resistance in Cancer Cells. Drug Delivery 2012, 19 (4), 169–176. [PubMed: 22506922]

(34). Krafft MP; Riess JG Chemistry, Physical Chemistry, and Uses of Molecular Fluorocarbon–Hydrocarbon Diblocks, Triblocks, and Related Compounds Unique “Apolar” Components for Self-Assembled Colloid and Interface Engineering. Chem. Rev 2009, 109 (5), 1714–1792. [PubMed: 19296687]

(35). Dai Z; Yao Q; Zhu L MMP2-Sensitive PEG–Lipid Copolymers: A New Type of Tumor-Targeted P-Glycoprotein Inhibitor. ACS Appl. Mater. Interfaces 2016, 8 (20), 12661–12673. [PubMed: 27145021]

(36). Dai Z; Tu Y; Zhu L Multifunctional Micellar Nanocarriers for Tumor-Targeted Delivery of Hydrophobic Drugs. J. Biomed. Nanotechnol 2016, 12 (6), 1199–1210. [PubMed: 27319214]

(37). Torchilin VP; Rammohan R; Weissig V; Levchenko TS Tat Peptide on the Surface of Liposomes Affords Their Efficient Intracellular Delivery Even at Low Temperature and in the Presence of Metabolic Inhibitors. Proc. Natl. Acad. Sci. U. S. A 2001, 98 (15), 8786–8791. [PubMed: 11438707]

(38). Shen Z; Ge J; Ye H; Tang S; Li Y Cholesterol-Like Condensing Effect of Perfluoroalkyl Substances on a Phospholipid Bilayer. J. Phys. Chem. B 2020, 124 (26), 5415–5425. [PubMed: 32515593]

(39). Leeb F; Maibaum L Spatially Resolving the Condensing Effect of Cholesterol in Lipid Bilayers. Biophys. J 2018, 115 (11), 2179–2188. [PubMed: 30447996]

(40). Rejman J; Bragonzi A; Conese M Role of Clathrin- and Caveolae-Mediated Endocytosis in Gene Transfer Mediated by Lipo- and Polyplexes. Mol. Ther 2005, 12 (3), 468–474. [PubMed: 15963763]

(41). Ivanov AI Pharmacological Inhibition of Endocytic Pathways: Is It Specific Enough to Be Useful? In Exocytosis and Endocytosis, Methods in Molecular Biology; Humana Press: Totowa, NJ, 2008; Vol. 440, pp 15–33.

(42). Kilsdonk EP; Yancey PG; Stoudt GW; Bangerter FW; Johnson WJ; Phillips MC; Rothblat GH Cellular Cholesterol Efflux Mediated by Cyclodextrins. J. Biol. Chem 1995, 270 (29), 17250–17256. [PubMed: 7615524]

(43). Chou LY; Ming K; Chan WC Strategies for the Intracellular Delivery of Nanoparticles. Chem. Soc. Rev 2011, 40 (1), 233–245. [PubMed: 20886124]

(44). Khalil IA; Kogure K; Akita H; Harashima H Uptake Pathways and Subsequent Intracellular Trafficking in Nonviral Gene Delivery. Pharmacol. Rev 2006, 58 (1), 32–45. [PubMed: 16507881]

(45). Varkouhi AK; Scholte M; Storm G; Haisma HJ Endosomal Escape Pathways for Delivery of Biologicals. J. Controlled Release 2011, 151 (3), 220–228.

(46). Kasuya MCZ; Nakano S; Katayama R; Hatanaka K Evaluation of the Hydrophobicity of Perfluoroalkyl Chains in Amphiphilic Compounds That Are Incorporated into Cell Membrane. J. Fluorine Chem 2011, 132 (3), 202–206.

(47). Yoder NC; Kalsani V; Schuy S; Vogel R; Janshoff A; Kumar K Nanoscale Patterning in Mixed Fluorocarbon– Hydrocarbon Phospholipid Bilayers. J. Am. Chem. Soc 2007, 129 (29), 9037–9043. [PubMed: 17602478]

(48). Koike S; Jahn R Probing and Manipulating Intracellular Membrane Traffic by Microinjection of Artificial Vesicles. Proc. Natl. Acad. Sci. U. S. A 2017, 114 (46), E9883–E9892. [PubMed: 29087339]

(49). Echevarría W; Leite MF; Guerra MT; Zipfel WR; Nathanson MH Regulation of Calcium Signals in the Nucleus by a Nucleoplasmic Reticulum. Nat. Cell Biol 2003, 5 (5), 440–446. [PubMed: 12717445]

(50). Lipsky NG; Pagano RE A Vital Stain for the Golgi Apparatus. Science 1985, 228 (4700), 745–747. [PubMed: 2581316]

(51). Marchi S; Patergnani S; Pinton P The Endoplasmic Reticulum–Mitochondria Connection: One Touch, Multiple Functions. Biochim. Biophys. Acta, Bioenerg 2014, 1837 (4), 461–469.

(52). Reers M; Smiley ST; Mottola-Hartshorn C; Chen A; Lin M; Chen LB Mitochondrial Membrane Potential Monitored by JC-1 Dye. Methods Enzymol. 1995, 260, 406–417. [PubMed: 8592463]

(53). Long L; Huang M; Wang N; Wu Y; Wang K; Gong A; Zhang Z; Sessler JL A Mitochondria-Specific Fluorescent Probe for Visualizing Endogenous Hydrogen Cyanide Fluctuations in Neurons. J. Am. Chem. Soc 2018, 140 (5), 1870–1875. [PubMed: 29337546]

(54). Krafft MP Fluorocarbons and Fluorinated Amphiphiles in Drug Delivery and Biomedical Research. Adv. Drug Delivery Rev 2001, 47 (2), 209–228.

(55). Hayakawa K; Esposito E; Wang X; Terasaki Y; Liu Y; Xing C; Ji X; Lo EH Transfer of Mitochondria from Astrocytes to Neurons after Stroke. Nature 2016, 535 (7613), 551–555. [PubMed: 27466127]

(56). Alleva R; Tomasetti M; Andera L; Gellert N; Borghi B; Weber C; Murphy MP; Neuzil J Coenzyme Q Blocks Biochemical but Not Receptor-Mediated Apoptosis by Increasing Mitochondrial Antioxidant Protection. FEBS Lett. 2001, 503 (1), 46–50. [PubMed: 11513852]

(57). Yamamoto S; Tamai H; Ishisaka R; Kanno T; Arita K; Kobuchi H; Utsumi K Mechanism of A-Tocopheryl Succinate-Induced Apoptosis of Promyelocytic Leukemia Cells. Free Radical Res. 2000, 33 (4), 407–418. [PubMed: 11022849]

(58). Temmerman K; Nickel W A Novel Flow Cytometric Assay to Quantify Interactions between Proteins and Membrane Lipids. J. Lipid Res 2009, 50 (6), 1245–1254. [PubMed: 19144996]

(59). Houtkooper R; Vaz F Cardiolipin, the Heart of Mitochondrial Metabolism. Cell. Mol. Life Sci 2008, 65 (16), 2493–2506. [PubMed: 18425414]

(60). Otsuka H; Nagasaki Y; Kataoka K PEGylated Nanoparticles for Biological and Pharmaceutical Applications. Adv. Drug Delivery Rev 2012, 64, 246–255.

(61). Klein E; Kerth P; Lebeau L Enhanced Selective Immobilization of Biomolecules onto Solid Supports Coated with Semifluorinated Self-Assembled Monolayers. Biomaterials 2008, 29 (2), 204–214. [PubMed: 17942149]

(62). Neuzil J; Tomasetti M; Zhao Y; Dong L-F; Birringer M; Wang X-F; Low P; Wu K; Salvatore BA; Ralph SJ Vitamin E Analogs, a Novel Group of 'Mitocans,' as Anti-Cancer Agents: The Importance of Being Redox-Silent. Mol. Pharmacol 2007, 71 (5), 1185–1199. [PubMed: 17220355]

(63). Neuzil J; Weber T; Schröder A; Lu M; Ostermann G; Gellert N; Mayne GC; Olejnicka B; Nègre-Salvayre A; Stícha M; et al. Induction of Cancer Cell Apoptosis by A-Tocopheryl Succinate: Molecular Pathways and Structural Requirements. FASEB J. 2001, 15 (2), 403–415. [PubMed: 11156956]

(64). Neuzil J; Dong L-F; Rohlena J; Truksa J; Ralph SJ Classification of Mitocans, Anti-Cancer Drugs Acting on Mitochondria. Mitochondrion 2013, 13 (3), 199–208. [PubMed: 22846431]

(65). Biswas S; Dodwadkar NS; Deshpande PP; Torchilin VP Liposomes Loaded with Paclitaxel and Modified with Novel Triphenylphosphonium-PEG-PE Conjugate Possess Low Toxicity, Target Mitochondria and Demonstrate Enhanced Antitumor Effects *in Vitro* and *in Vivo*. J. Controlled Release 2012, 159 (3), 393–402.

(66). Dong L-F; Freeman R; Liu J; Zobalova R; Marin-Hernandez A; Stantic M; Rohlena J; Valis K; Rodriguez-Enriquez S; Butcher B; et al. Suppression of Tumor Growth *in Vivo* by the Mitocan A-Tocopheryl Succinate Requires Respiratory Complex Ii. Clin. Cancer Res 2009, 15 (5), 1593–1600. [PubMed: 19223492]

(67). Qi Y; Song H; Xiao H; Cheng G; Yu B; Xu FJ Fluorinated Acid-Labile Branched Hydroxyl-Rich Nanosystems for Flexible and Robust Delivery of Plasmids. Small 2018, 14, 1803061.

(68). Friedrich J; Seidel C; Ebner R; Kunz-Schughart LA Spheroid-Based Drug Screen: Considerations and Practical Approach. Nat. Protoc 2009, 4 (3), 309–324. [PubMed: 19214182]

(69). Liu Y; Wang J; Zhang J; Marbach S; Xu W; Zhu L Targeting Tumor-Associated Macrophages by MMP2-Sensitive Apoptotic Body-Mimicking Nanoparticles. ACS Appl. Mater. Interfaces 2020, 12 (47), 52402–52414. [PubMed: 33169982]

(70). Wallace DC Mitochondria and Cancer. Nat. Rev. Cancer 2012, 12 (10), 685–698. [PubMed: 23001348]

(71). Whiteside T The Tumor Microenvironment and Its Role in Promoting Tumor Growth. Oncogene 2008, 27 (45), 5904–5912. [PubMed: 18836471]

(72). Pulaski BA; Ostrand-Rosenberg S Mouse 4T1 Breast Tumor Model. Curr. Protoc. Immunol 2000, 39, 20.2.1–20.2.16.

(73). Yao Q; Liu Y; Kou L; Tu Y; Tang X; Zhu L Tumor-Targeted Drug Delivery and Sensitization by MMP2-Responsive Polymeric Micelles. Nanomedicine 2019, 19, 71–80. [PubMed: 31004812]

(74). Liu Z; Chen K; Davis C; Sherlock S; Cao Q; Chen X; Dai H Drug Delivery with Carbon Nanotubes for *in Vivo* Cancer Treatment. Cancer Res. 2008, 68 (16), 6652–6660. [PubMed: 18701489]

(75). Working PK; Newman MS; Johnson J; Cornacoff JB Safety of Poly(ethylene Glycol) and Poly(ethylene Glycol) Derivatives. In Poly(ethylene Glycol); American Chemical Society: Washington, DC, 1997; Vol. 680, pp 45–57.

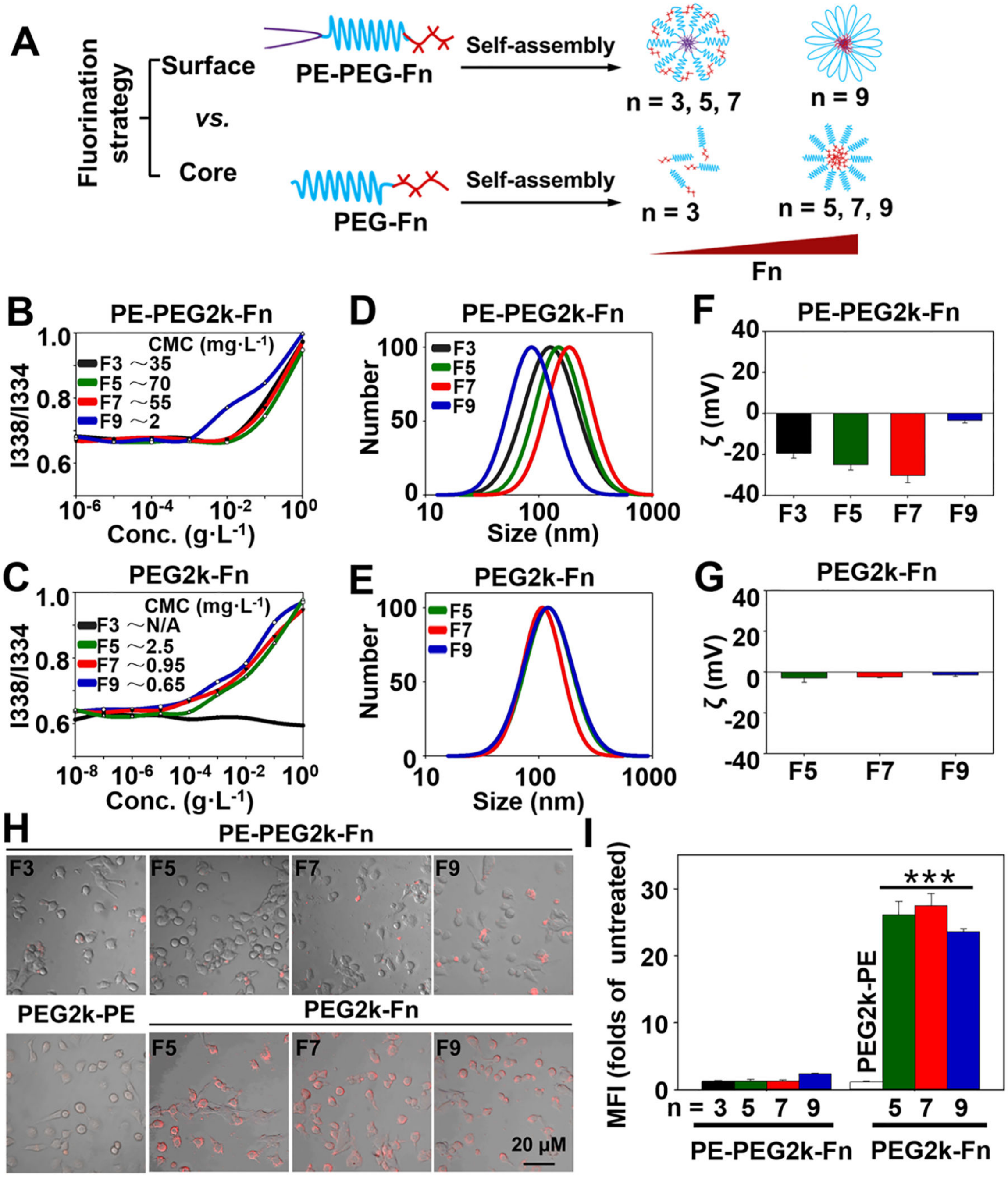

Figure 1.

Fluorination strategies of the self-assembled micellar nanoparticles. (A) Scheme of the fluorination strategies and fluoroamphiphiles' self-assembly patterns. (B, C) CMC values determined using the pyrene as a fluorescent probe. (D, E) Particle sizes of the polymeric micelles (pH 7.4) determined by dynamic light scattering (DLS). (F, G) ζ potentials of the polymeric micelles (pH 7.4). Cellular uptake of the Rh-PE-labeled micelles in the HeLa cells determined by (H) fluorescence microscopy and (I) flow cytometry. Incubation time: 1

h. MFI, mean fluorescence intensity. Data were expressed as the mean ± SD, ***$p < 0.001$, when compared to the PE-PEG2k-Fn groups or PEG2k-PE group.

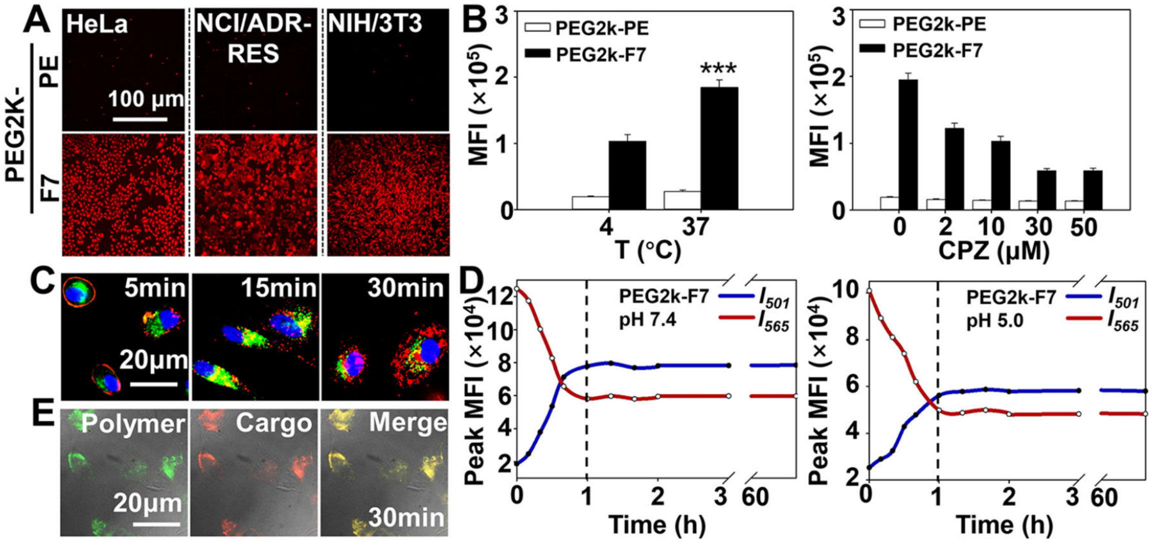

Figure 2.

Cellular uptake and intracellular delivery. (A) Cellular uptake of the Rh-PE-labeled micelles. Incubation time: 1 h. (B) Effects of the temperature and endocytosis inhibitor on cellular uptake, determined by flow cytometry. For the endocytosis inhibition study, the cells were preincubated with the chlorpromazine (CPZ) for 0.5 h and then incubated with the Rh-PE-labeled micelles for an additional hour. (C) Endocytosis and endosomal escape. Cell nuclei were stained by the Hoechst 33258 (blue). Endolysosomes were stained by the LYSO-ID Green. (D) Fusion of the 1,2-dipalmitoyl-*sn*-glycerol-3- phosphocholine liposomes in the presence of the polymers, determined by the FRET (dye pair: DiI/DiO). The protocol is depicted in Figure S2A,B. (E) Cellular tracking of the Rh-PE loaded FITC-PEG2k-F7 micelles. Incubation time: 0.5 h. MFI, mean fluorescence intensity. Cell line in (B), (C) and (E): HeLa cells. Data were expressed as the mean ± SD, $^{***}p < 0.001$, when compared to the PEG2k-F7 group at 4 °C.

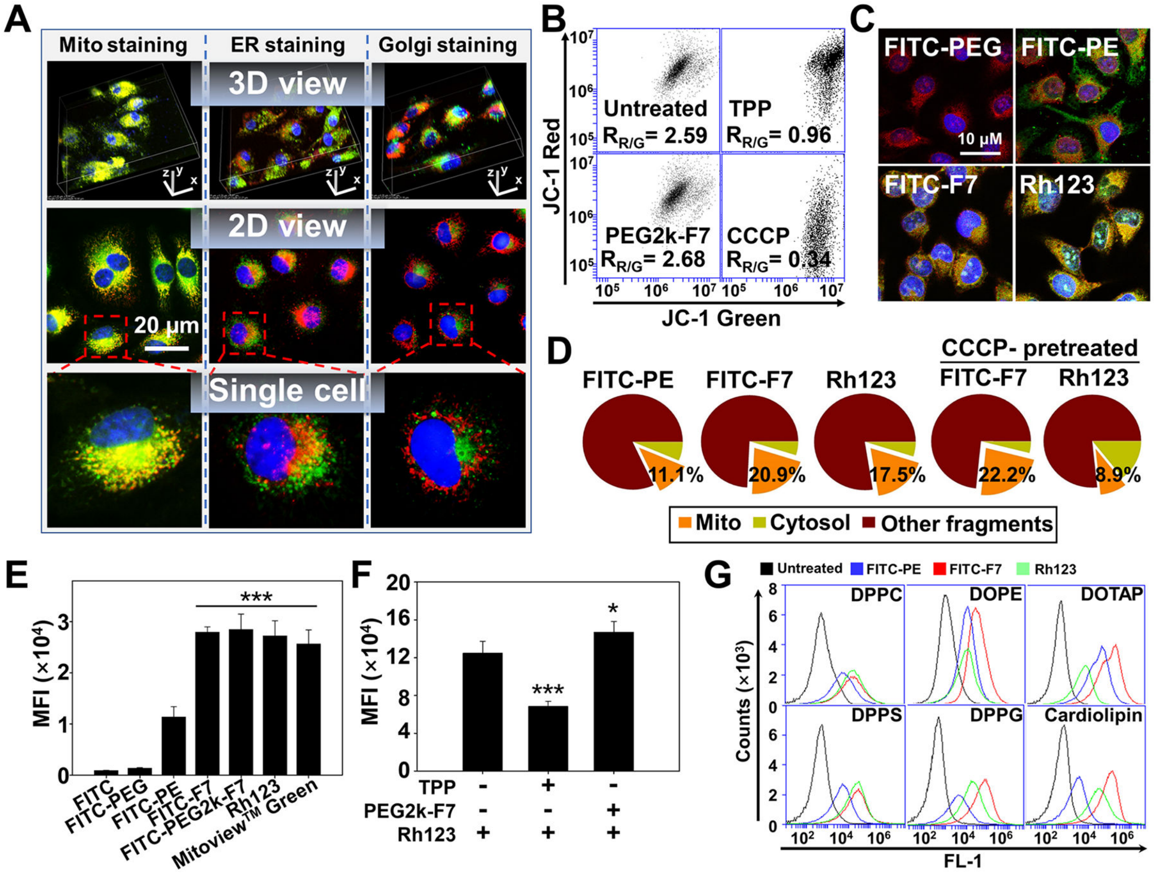

Figure 3.

Potential-independent mitochondrial targeting. (A) Intracellular localization of the Rh-PE-labeled micelles. Incubation time: 1 h. Mitochondria were stained by the MitoView Green. ER was stained by the ER-Tracker Green. Golgi apparatuses were stained by the NBD C6-ceramide. Mitochondria, ER, and Golgi showed green fluorescence. Cell nuclei were stained by the Hoechst 33258 (blue). (B) Mitochondrial membrane potential determined by the JC-1 dye. The decrease in the red/green ratio ($R_{R/G}$) indicates the mitochondrial depolarization. (C) Colocalization of the FITC-labeled materials with mitochondria. Incubation time: 1 h. Mitochondria were stained by the MitoView 633 (red). (D) Quantification of the mitochondria-associated polymers. The cells were incubated with the FITC-labeled polymers for 1 h, followed by the mitochondrial isolation and fluorescence quantitation. To study the influence of the mitochondrial depolarization, the cells were preincubated with the CCCP for 15 min before 1 h polymer incubation. (E) Direct binding affinity. The isolated mitochondria were incubated with the FITC-labeled polymers or dyes at 37 °C for 1 h. The mitochondria-associated fluorescence was quantitated. (F) Competitive binding assay. The isolated mitochondria were preincubated with either the TPP or PEG2k-F7 at 37 °C for 1 h, followed by incubation with the Rh123 for 1 h. The mitochondria-associated Rh123 was quantitated. (G) Polymer–lipid binding. The liposomes were incubated with the FITC-labeled polymers or Rh123 at 37 °C for 1 h, followed by flow cytometry. MFI, mean fluorescence intensity. Cell line in (A–D): HeLa cells. Data were expressed as the mean ±

SD, ***$p < 0.001$, when compared to the FITC, FITC-PEG, or FITC-PE (E), *$p < 0.05$; ***$p < 0.001$, when compared to the Rh-PE group in the absence of polymers (F).

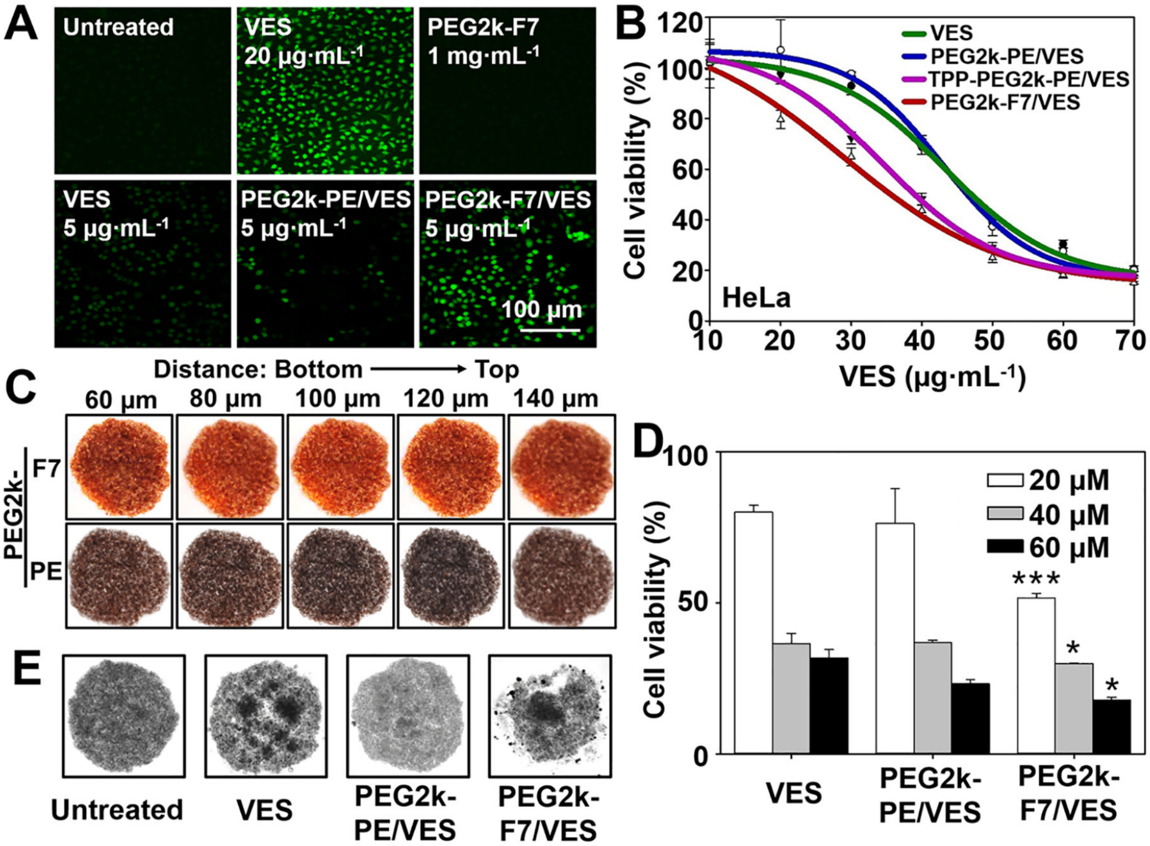

Figure 4.

In vitro drug delivery. (A) Cellular ROS levels. Cells were incubated with various formulations for 20 h, and then incubated with the H_2DCFDA (10 μM) at 37 °C for 0.5 h. The generated green fluorescence, an indicator of the ROS, was determined by fluorescence microscopy. (B) Cytotoxicity of the VES-loaded micelles determined by the CellTiter-Blue Cell Viability assay. Incubation time: 48 h. (C) Penetration of the Rh-PE-labeled micelles in the cell spheroids. Incubation time: 1 h. (D) Cytotoxicity and (E) spheroid morphology upon treatments in the cell spheroids. Incubation time: 72 h. Cell line: HeLa cells. Data were expressed as the mean ± SD, *$p < 0.05$; ***$p < 0.001$, when compared to the PEG2k-PE/VES group.

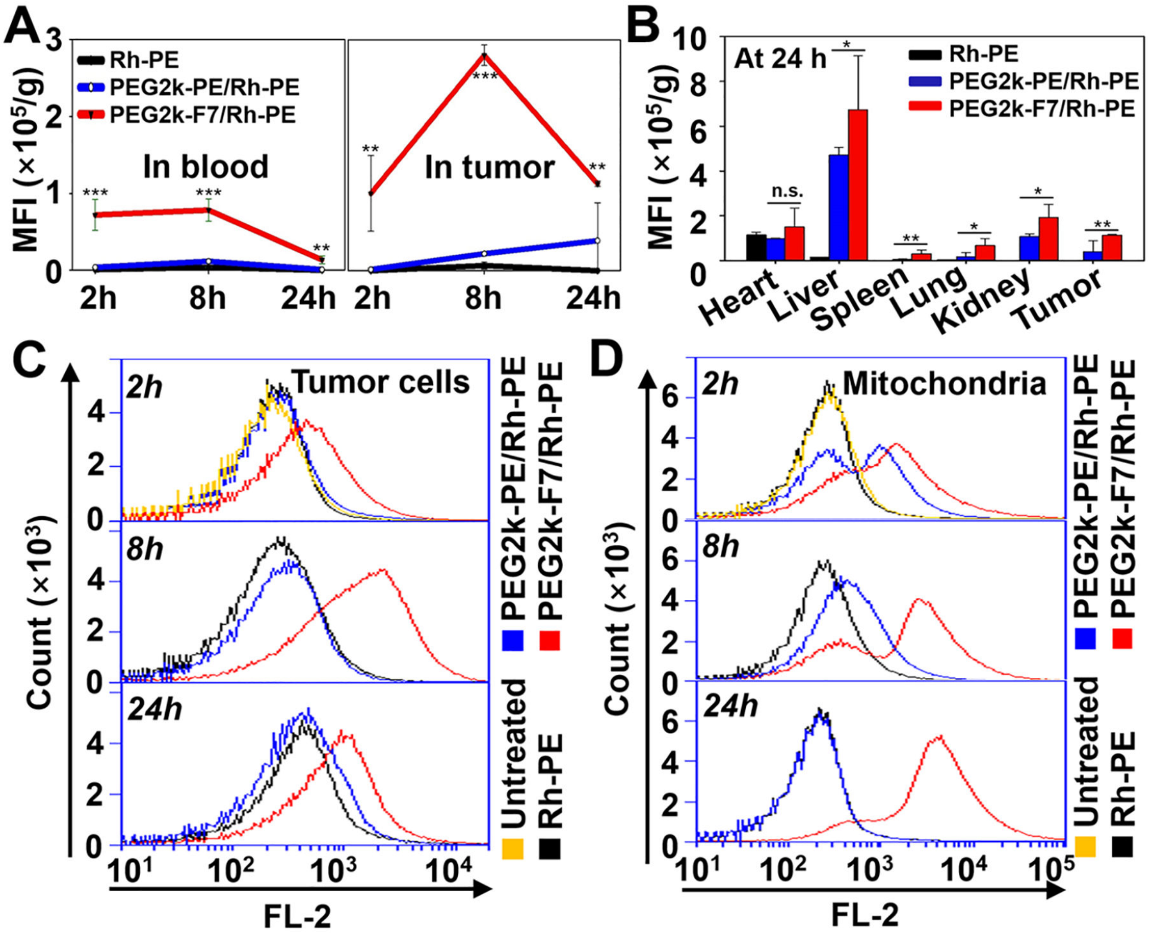

Figure 5.

In vivo biodistribution, cellular uptake, and mitochondrial accumulation. Biodistribution of the Rh-PE-labeled micelles in the blood and tumor over 24 h (A) and in the major organs and tumor at 24 h (B). (C) Internalization of the Rh-PE-labeled micelles by the tumor cells, determined by flow cytometry. (D) Accumulation of the Rh-PE-labeled micelles in the tumoral mitochondria, determined by flow cytometry. Animal model: 4T1-bearing BALB/c mice. Administration: single i.v. injection through the mouse tail vein. Data were expressed as the mean ± SD, $*p < 0.05$; $**p < 0.01$; $***p < 0.001$; n.s., nonsignificant, when compared to the PEG2k-PE/Rh-PE group.

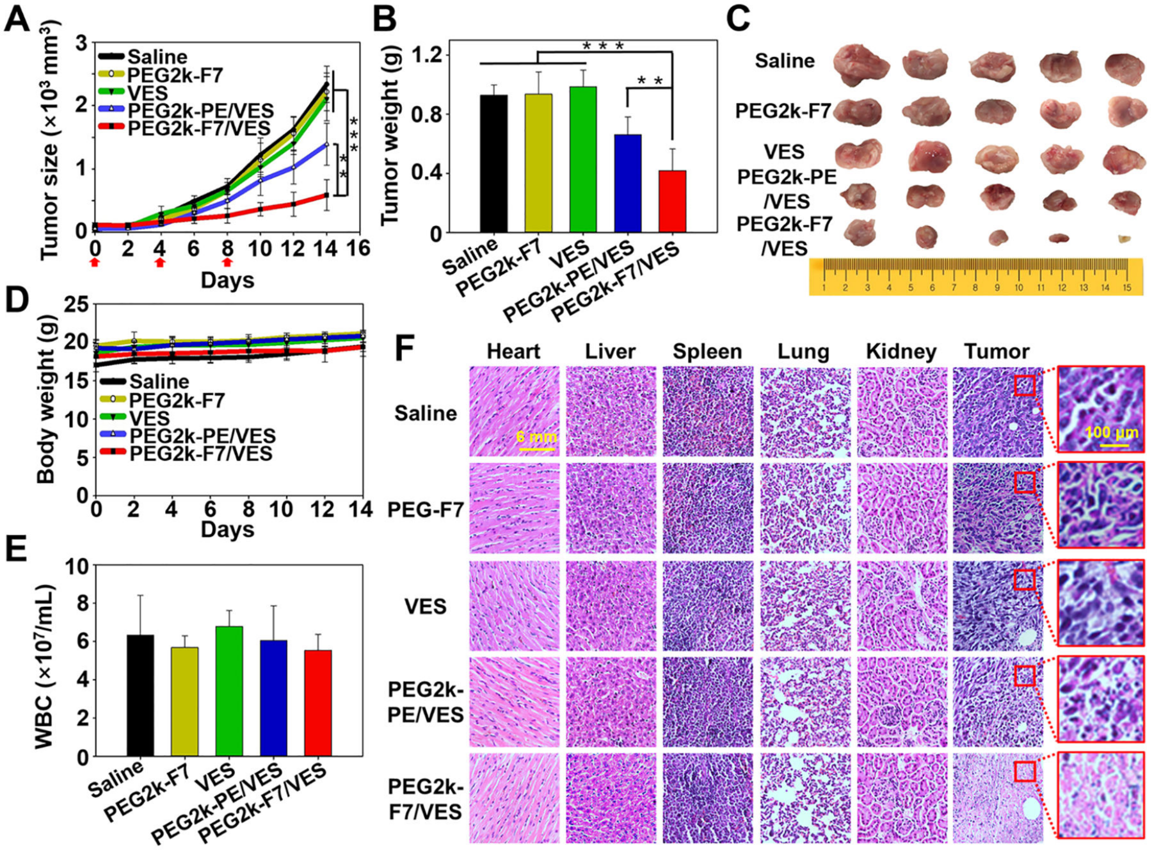

Figure 6.

In vivo anticancer activity. (A) Tumor growth curves. (B) Weights and (C) images of the excised tumors on day 14. (D) Mouse body weights. (E) White blood cell counts. (F) H&E staining of the vital organs and tumors. Animal model: 4T1-bearing BALB/c mice. Administration: i.v. injection through the mouse tail vein at 20 mg·kg^{-1} VES every 4 days for three times. Data were expressed as the mean ± SD, $^{**}p < 0.01$; $^{***}p < 0.001$.